

N 9 1 - 3 0 2 3 5

Significant Reduction in Arc Frequency of Negatively Biased Solar Cells:  
Observations, Diagnostics, and Mitigation Technique(s)

B.L. Upschulte, G.M. Weyl, and W.J. Marinelli  
Physical Sciences Inc.  
Andover, Massachusetts

E. Aifer  
Boston University  
Boston, Massachusetts

D. Hastings  
Massachusetts Institute of Technology  
Cambridge, Massachusetts

D. Snyder  
NASA LeRC

A variety of experiments have been performed which identify key factors contributing to the arcing of negatively biased high voltage solar cells. These efforts have led to reduction of greater than a factor of 100 in the arc frequency of a single cell following proper remediation procedures. Experiments naturally lead to and focussed on the adhesive/encapsulant that is used to bond the protective cover slip to the solar cell. An image-intensified CCD camera system recorded UV emission from arc events which occurred exclusively along the interfacial edge between the cover slip and the solar cell. Microscopic inspection of this interfacial region showed a bead of encapsulant along this entire edge. Elimination of this encapsulant bead reduced the arc frequency by two orders of magnitude.

Water contamination has also been identified as a key contributor which enhances arcing of the encapsulant bead along the solar cell edge. Spectrally resolved measurements of the observable UV light shows a feature assignable to OH(A-X) electronic emission, which is common for water contaminated discharges. Experiments in which the solar cell temperature was raised to 85°C showed a reduced arcing frequency, suggesting desorption of H<sub>2</sub>O. Exposing the solar cell to water vapor has been shown to increase the arcing frequency. Clean dry gases such as O<sub>2</sub>, N<sub>2</sub>, and Ar show no enhancement of the arcing rate. Elimination of the exposed encapsulant eliminates any measurable sensitivity to H<sub>2</sub>O vapor.

#### INTRODUCTION

The demands on future space power systems encourage all of us to investigate every possible avenue to increase output power, reduce weight, and improve efficiency. High voltage arrays, i.e., several hundred volts, have the distinct advantage of higher output power with minimal design changes and little weight penalty. Unfortunately, high voltage arrays exhibit undesirable arcing phenomena. In particular, for negatively biased solar cell arrays this arcing leads to disruptive RF noise, and may potentially damage sensitive electronic components or the solar array itself. It has been experimentally observed (Refs. 1 through 6) that arcing begins at bias voltages more negative than -300V. Although several mechanisms have been suggested to explain the

arcing phenomena/behavior, very little hard evidence is available which unambiguously identifies the physical processes which control arc initiation or maintenance.

In this paper we will describe a set of experiments which identify key factors contributing to arcing of negatively biased solar cells. We begin by describing the unique ultra-high vacuum plasma test facility and its performance characteristics. Following this we will describe several arc diagnostics which were instrumental in our findings; then we will describe in detail the most relevant measurements, observations, and analysis. In our conclusion, we will suggest future mitigation techniques to make high voltage solar cell arrays of practical use, and suggest complimentary testing techniques to identify the microscopic mechanism associated with arcing.

## APPARATUS

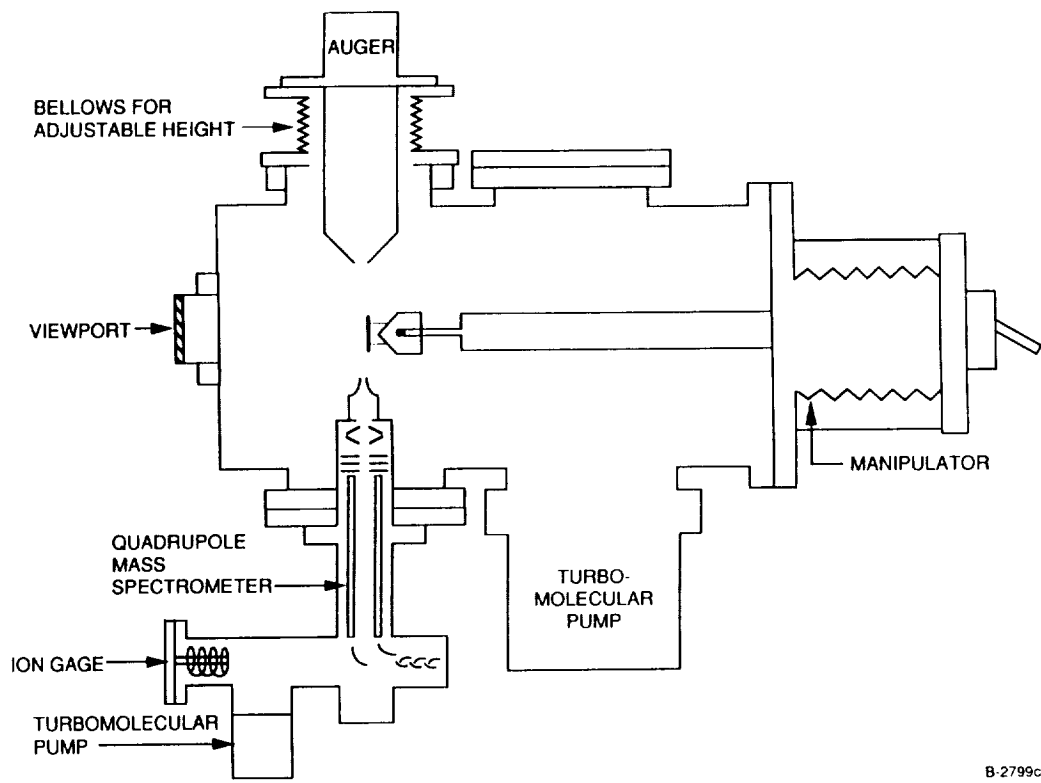
All experiments were conducted in an ultra-high vacuum (UHV) chamber. The chamber is a 21 in. long by 10 in. o.d. cylinder in which all ports are sealed with Cu gaskets and knife edge flanges to allow operation at pressures as low as  $2 \times 10^{-11}$  torr. The chamber is shown schematically in Figure 1 and described below. In the forward section of the chamber are four 6-in. clear aperture ports employed for operation of sample diagnostics. An Auger electron spectrometer is located on the top flange and may be positioned to within 0.25 in. of the sample for surface analysis. A differentially pumped quadrupole mass spectrometer (0 to 300 amu range) is located on the lower port and is configured to detect species desorbed from the sample as well as the background environment. Ports on either side of the chamber and on the end wall are available for optical access. In these experiments the end wall port is used for optical access and may be equipped with a fast, low resolution optical spectrometer for discharge characterization. A camera system may be employed to photograph arcing events from this port as well. One of the side ports is fitted with the plasma source. The end-wall of the chamber may also be equipped with a retarding potential electron energy analyzer which may be employed to sample emission from the surface. The side ports were used to support retractable planar and cylindrical Langmuir probes.

In the mid-section of the chamber four small access ports are provided for pressure measurement (ionization gauge), gas dosing, and a 0 to 5 keV ion sputtering gun for sample cleaning. In the rear section of the chamber, ports are provided for a 1000 1/s turbomolecular pump and sample viewing.

The samples to be tested are mounted in the cradle of a 5 degree-of-freedom sample manipulator which provides access to all of the forward ports in the chamber. High voltage and low-voltage isolated feedthroughs are used for precise electrical measurements.

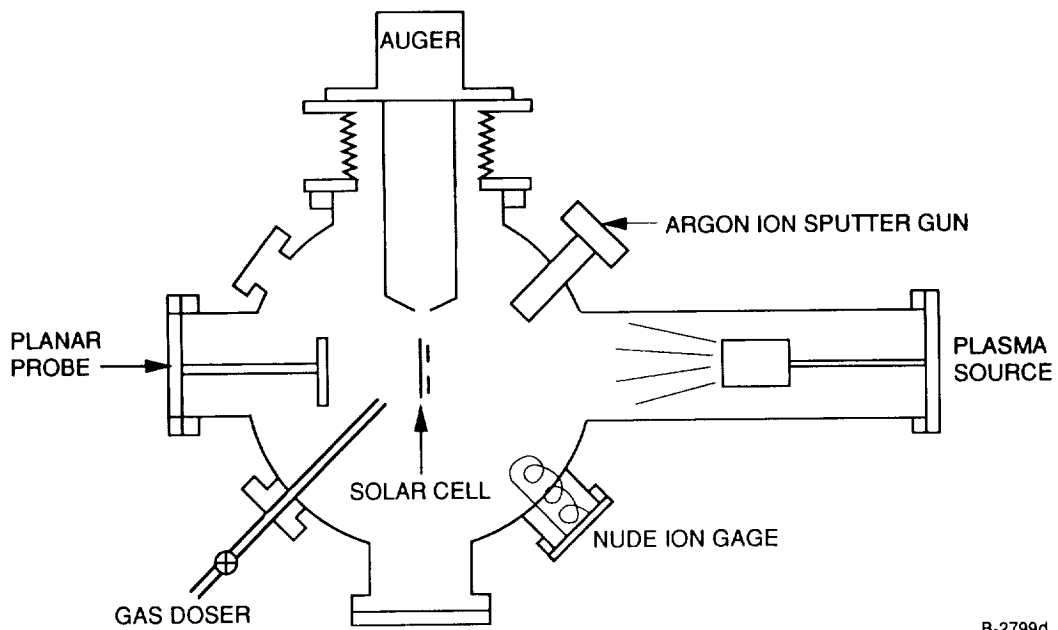
The plasma source is a 3 cm Kaufmann type charge-neutralized ion source purchased from Ion Tech Inc. It has been mounted on a vacuum flange and slides into a full nipple extension attached to an 8 in. conflat flange port on the UHV chamber. The plasma source mounting bracket slides on threaded rods to allow the source to solar cell distance to be varied from 13 to 35 cm. The three rods are arranged in an optical mount pattern so that small angular adjustments may be specifically and reproducibly set. Argon plasmas are typically used in our measurements. The flow of argon used during plasma source operation is roughly 1 sccm and produces a chamber pressure of  $1 \times 10^{-5}$  torr. Although this argon pressure is relatively high, the largest partial pressure of a contaminant is  $\leq 1 \times 10^{-7}$  torr. This background pressure is due to  $H_2O$  desorbed from the chamber walls when the hot Kaufmann ion source is in operation. Typical plasma densities are presented in Table 1. The electron temperature was found to be  $1.25 \text{ eV} \pm 0.15 \text{ eV}$ . Samples were positioned 25 cm downstream from the plasma source. The radial profile of the ion beam at this position was measured using the cylindrical Langmuir probe in ion saturation mode. Figure 2 shows the size of the ion beam, full width at half maximum, to be at least 5 cm, i.e., larger than the sample solar cells used in our measurements.

Several diagnostics played a crucial role in these experiments. A capacitively coupled current sensor based on an experimental design by Snyder<sup>3</sup> was utilized for all measurements, and provided a master trigger signal for many of the other diagnostics. A high voltage probe (Tektronix Model P6015) was attached to the solar cell interconnect to monitor time dependent voltage variations during arc events. Time bandwidths in excess of 8 MHz were realizable with the voltage probe, and bandwidths in the range of 100 MHz were



(a) Side View

B-2799c



(b) View Along Manipulator Axis

B-2799d

Figure 1. - Schematic drawing of the UHV chamber showing location of diagnostics.

TABLE 1. - PLASMA CHARACTERISTICS

Beam Energy (eV)	Electron Density ( $10^6 \text{ cm}^{-3}$ )	Ion Density ( $10^6 \text{ cm}^{-3}$ )
20	$7.4 \pm 1.5$	$5.6 \pm 1.0$
30	7.4	5.5
40	8.8	6.0
50	10.0	7.5
60	12.1	10.0

obtainable with the current sensor. A UV radiometer was implemented and viewed arc events through the end viewport. This device consisted of a Hamamatsu Model R1220 solar blind photomultiplier tube in an EMI-Gencom Model SRI/F housing. This tube provides an active photocathode of about 3/4 in. in diameter and response from the air transmission cutoff at, around 190 nm, to 305 nm with a quantum efficiency of approximately 0.2. The same UV light was spectrally resolved using a Princeton Instruments Optical Multichannel Analyzer (OMA) coupled to a Jarrell-Ash 1/4 meter monochromator. The dispersed light from the monochromator's 300 line/mm grating is detected on a 712 element diode array. The multiplex advantage of the OMA allows simultaneous detection of all light throughout the 200 to 400 nm region for each arc event. The diagnostic most useful in our measurements is a unique PSI designed and

built intensified CCD camera system. The CCD array is a Model NXA 1060 by Amperex and is coupled to a Nikon F/4.5 compound quartz lens system. Custom gating circuitry and software allowed us to trigger the gated image intensifier with the current sensor. Using a UG-5 ultraviolet filter, we were able to capture arc emission in a  $5 \mu\text{s}$  gate width. Actual images of individual arc events were displayed in false color video format. Finally, we made excellent use of an Olympus Model BH2 phase sensitive microscope to inspect and photograph changes in the solar cell edges.

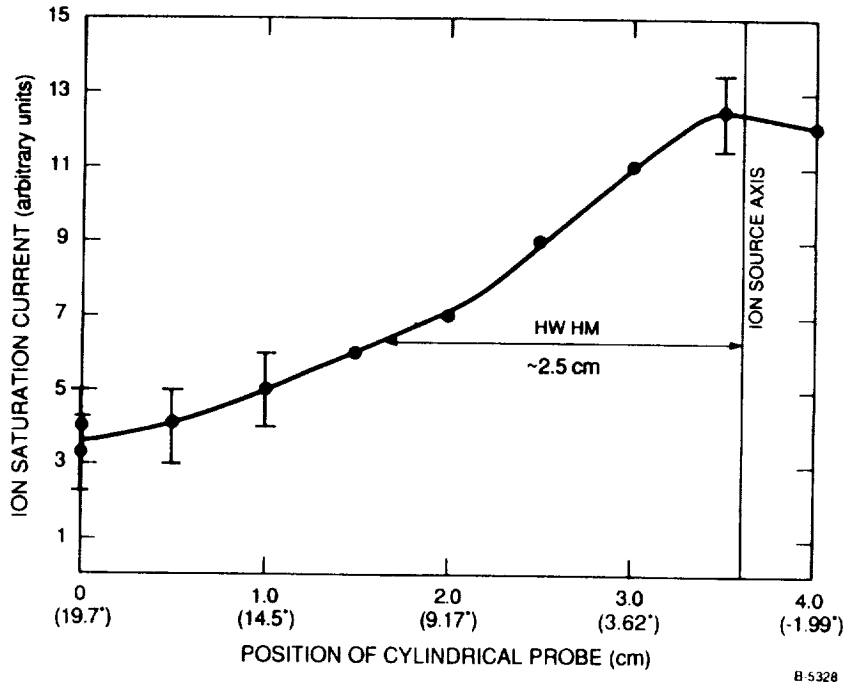


Figure 2. - Radial profile of ion saturation current, cylindrical probe.

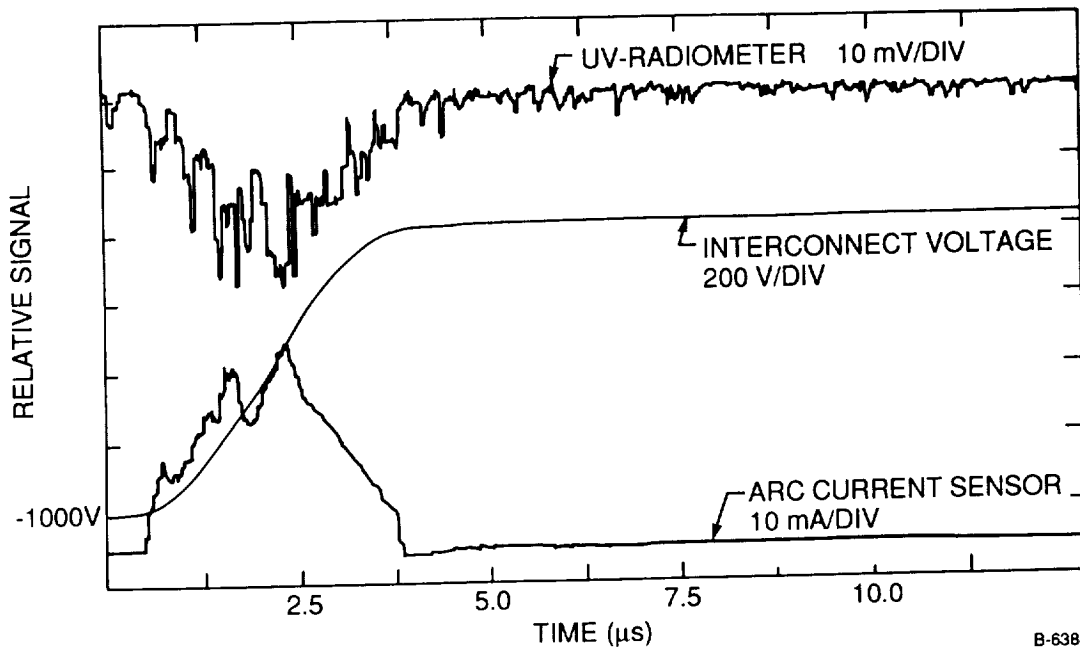
Experimental Observations

The relevant experiments to be described below were performed on "thin" solar cells, (i.e.,  $\sim 250 \mu\text{m}$  thick) provided to us by Spectralab, Inc. These cells measured  $2 \times 1 \text{ cm}^2$  and had silica cover plates that extended beyond the edge of the cell on all sides by approximately  $100 \mu\text{m}$ . The cells were mounted individually on the manipulator, where they were exposed to the plasma from the ion source. High voltage leads, which were determined to be free of arcing sites, were used to bias the solar cell to the test voltages. Plasma ion energies for all these tests reported here were 40 eV, and most tests were performed at a cell bias of -1000V.

A lengthy set of initial electrical/optical correlations were first measured to confirm that the UV light emission arises from the arc event. Figure 3 presents digitized oscilloscope traces of the UV Radiometer, the high voltage probe, and the current sensor. It is immediately obvious that the UV emission and the instantaneous current are extremely well correlated. A running integral of the current has been shown to produce a curve matching the interconnect voltage change as prescribed by  $dQ = CdV$ . In fact, a very accurate measurement of the sensor capacitance can be obtained from this linear relationship. In addition, we found the integral of the UV light emission was well correlated with the interconnect voltage change as well.

Polaroid pictures of the CCD camera images, as displayed on the computer screen, are used for the presentation of the observed arc event. The images are false color encoded and the brighter total emission level corresponds to the white regions of the picture while the blue-black color corresponds to the lower light emission regions. Figure 4 shows a full screen picture of an arc event. The entire profile of the solar cell is observable. The solar cell interconnect is located at the right edge. The brighter line observed along this edge of the cell is the result of light from the arc event scattering off of the embedded interconnect. All arc events occurred at the lower edge of the solar cell, not in the interconnect region. This entire lower edge is a triple junction point due to the silver conducting film on the bottom of the solar cell and due to the dielectric adhesive extruded along this edge as a result of attaching the cover slip to the cell. The luminosity dispersed around the cell arises due to light scattered off the Kovar interconnect/support. The white center of the arc is sufficiently bright to bleach/bleed across to other pixels on the CCD array and should not be interpreted as a measurement of the size of the arc spot. Arc spots have been measured as small as  $200 \mu\text{m}$ , but most measurements suggest the characteristic size of the spot to be order of  $500 \mu\text{m}$ . Although many images of arc events were acquired, we never observed detectable light emission at any location other than at this lower edge of the solar cell.

Our observation led us to examine the lower edge region of the cell where arc events had been recorded. Upon inspection, we observed a bead of adhesive along this edge; apparently squeezed out from between the silicon and cover slip during assembly. We did not observe any indication of damage due to the arc events or any unique site that might have been responsible for the large frequency of arc events at this edge. Indeed, the inspection of all the edges appeared very similar. Our next inclination was to inspect a new solar cell which had never been exposed to the plasma. This cell showed an identical accumulation of adhesive as observed for the plasma irradiated cell. An example picture (X50) is shown in Figure 5. This photo concentrates



B-6380

Figure 3. - Time-resolved record of current flow, voltage change, and UV emission during an arc event.

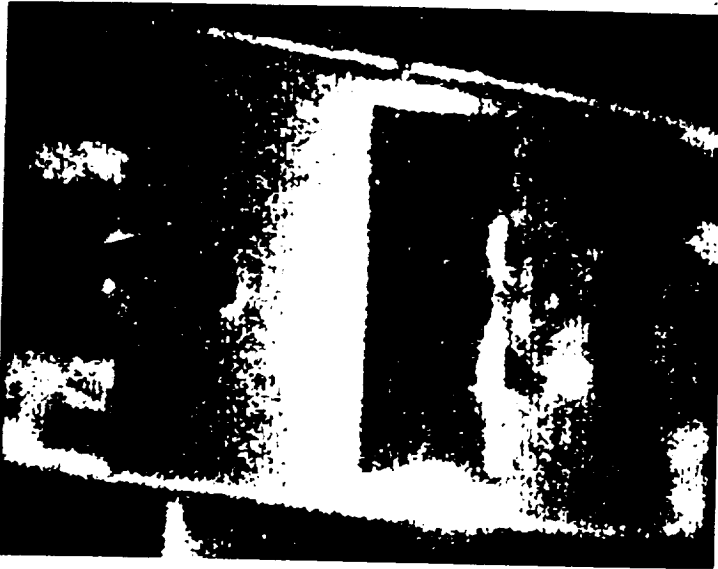


Figure 4. - CCD camera image of a solar cell arc event.

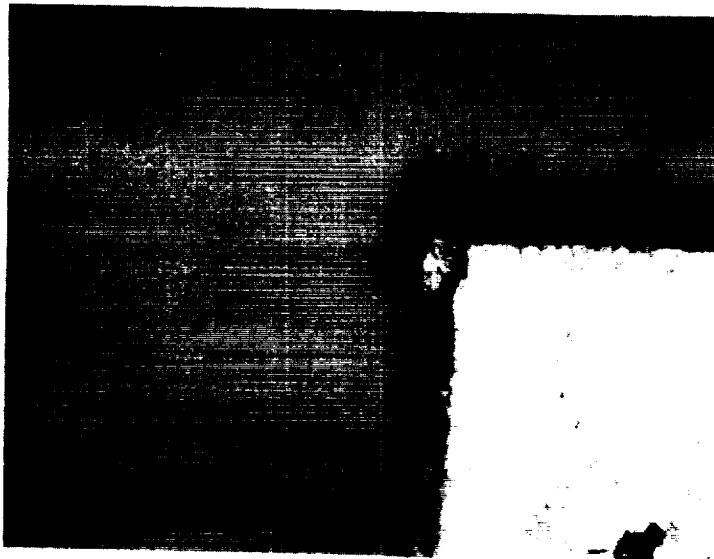


Figure 5. - Exposed adhesive/encapsulant along the edge and corner of the solar cell.

filament but no plasma exposure. The cell was then exposed to the plasma and arcing rate measurements were performed. The results of 40 min and 3 hr of heating are shown in Figure 7. These experiments clearly demonstrate that the arcing rate is dependent upon the time spent by the cell at elevated temperatures, where the outgassing rates are greatest. In these experiments the cell is not exposed to the plasma during the heating period. Hence, the reduction in arcing rate can clearly be correlated with a temperature increase rather than

on a corner of this particular solar cell, where a substantial amount of adhesive is observed. The adhesive edge displays both flake-like and globular structures. The adhesive is clear to opaque and difficult to discern on normal contrast film. The phase sensitive polarizer of the microscope was utilized to invert the contrast, making the adhesive look dark. Some flakes are quite large, on the order of 10 to 100  $\mu\text{m}$ . In a variety of places filaments or hairlike fibers of adhesive were observed to be protruding from the edges. These features are much smaller and particularly difficult to photograph because of magnification, depth of field, and contrast problems.

During the course of many of our experiments, we had observed the arcing rate decrease with continual exposure to the plasma. At first we believed this to be an irreversible morphology change in the triple junction region due to the plasma coupling current. Later we observed that the arc frequency would recover to a higher arc rate after cycling the vacuum system to atmosphere and back to  $10^{-9}$  torr. We also performed some experiments to monitor the temperature of the support plate and the Kovar interconnect during the plasma exposure period. The results of these experiments are shown in Figure 6. This chart plots the arc frequency on a log scale versus the cumulative plasma exposure time on the horizontal axis (bottom) and cross correlates that exposure time with the interconnect temperature shown on the top horizontal axis. The interconnect temperature rises due to the radiative heating from the plasma neutralizing filament. The arc rate is observed to decrease with time/temperature. Several experiments were then conducted to investigate this phenomenon. First, following an atmosphere to vacuum cycling, the solar cell was subjected to only the radiative heating due to the

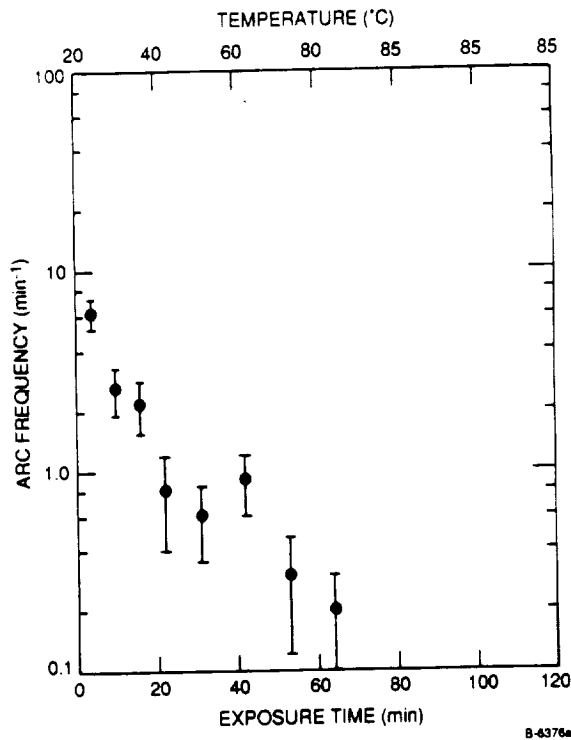


Figure 6. - Arc frequency versus plasma exposure time.

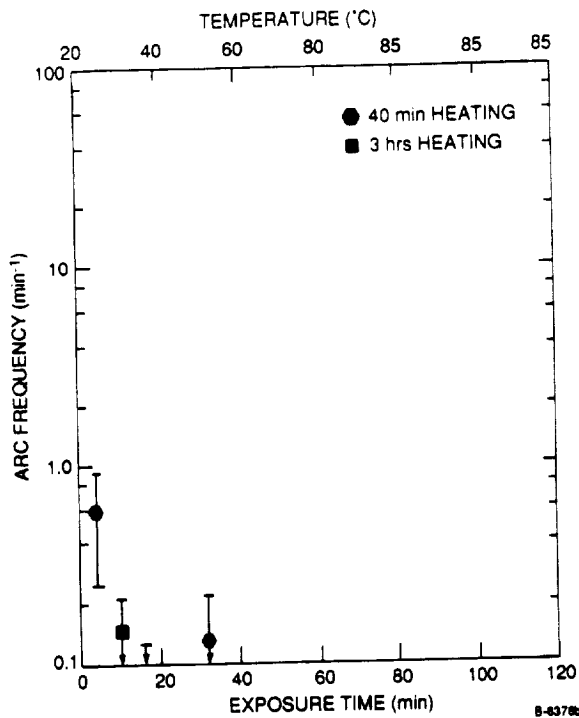


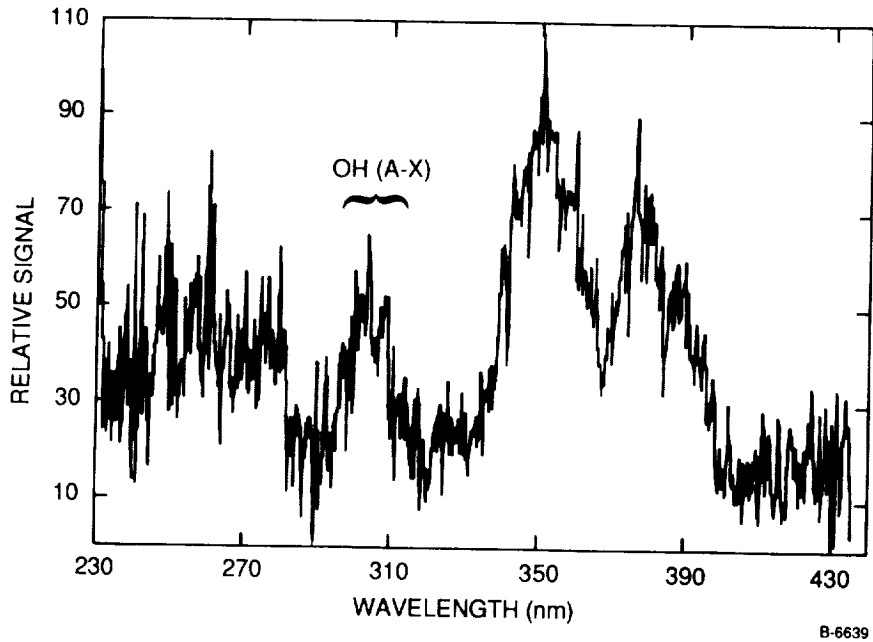
Figure 7. - Arc frequency after solar cell heating.

plasma exposure. Furthermore, upon cooling the cell to room temperature, this reduced arcing rate persists for a period of several hours to as long as 2 days. During this time the cell slowly readsorbs ambient water vapor in the UHV chamber (base pressure  $10^{-9}$  torr) and the arcing rate will slowly rise to the rate observed upon initially placing the cell into the chamber. Hence, the role of temperature in controlling the arcing rate is through its effect on adsorbate vapor pressures. This hypothesis was further confirmed in our next set of experiments.

In this experiment we used the OMA to spectrally resolve the arc emission. The spectra shown in Figure 8 suffers from poor signal-to-noise levels, but clearly shows the presence of the  $\text{OH}(A^2\Sigma v'=0 - X^2\Pi v''=0)$  feature at 306 nm. This feature is commonly observed in all types of electrical discharges contaminated with water.

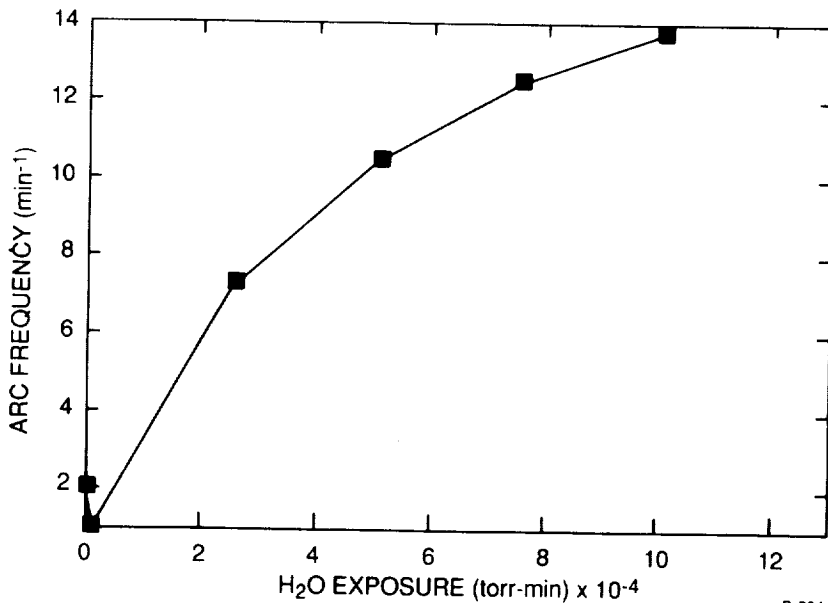
The larger features at 350 and 380 nm cannot be uniquely identified at this low signal level and poor resolution. Possible contributors are  $\text{AgO}$ ,  $\text{Fe}$ , and  $\text{CN}$ . Some of the features below 290 nm are suspected to be  $\text{NO}(A^2\Sigma - X^2\Pi) \gamma$  or  $(B^2\Pi - X^2\Pi) \beta$  bands, but once again the poor signal and resolution prohibit a unique identification.

Our next set of experiments investigated arc frequency with controlled exposure to likely adsorbates. Mass spectrometer measurements in our UHV chambers suggested the most ubiquitous contaminant is water. We controlled the temperature of the solar cell with the radiative heat load of the neutralizing filament, then exposed the solar cell to varying amounts of water vapor using a variable leak valve and reservoir of distilled degassed water. The arc frequency was observed to increase with additional exposure to the  $\text{H}_2\text{O}$  vapor. The data is shown in Figure 9. The  $\text{H}_2\text{O}$  exposure is cumulative, with the step size of the exposures being  $2.5 \times 10^{-4}$  torr-min. The arc frequency is determined with three consecutive 2-min counts of the observed arcs using the capacitively coupled sensor. Radiative heating was continued through the  $\text{H}_2\text{O}$  exposure period to maintain the temperature near  $80^\circ\text{C}$ . Analysis of this data suggests the arc rate increases with the 0.6 power of the dosing of  $\text{H}_2\text{O}$  on the solar cell. One might expect the arc frequency to



B-6639

Figure 8. - Spectra of solar cell arc emission at 8 nm resolution.



B-6644

Figure 9. - Arc frequency of heated solar cell as a function of cumulative H<sub>2</sub>O exposure.

increase with H<sub>2</sub>O dosing to the first power. This would resemble the adsorption of a contaminant with negligible desorption during the measurement. Our measured 0.6 power dependence is most likely the result of some desorption occurring during the period of the experimental measurement. The desorption of H<sub>2</sub>O contamination from the cell surface should be quite rapid at elevated temperatures. The apparent arcing rate observed in these measurements does not reflect this type of desorption phenomenon. Rather, the experiments suggest that H<sub>2</sub>O

is absorbed in depth into the adhesive. Under these conditions the arcing rate is a function of the temperature-dependent diffusion rate of absorbed  $H_2O$  into the material. This observation is consistent with the properties of the adhesive used to attach the protective cover slip to the cell surface. As applied, these epoxies are hydrophilic and often contain metallic impurities. As a cross check, the same solar cell was exposed to clean dry gases, i.e., argon, oxygen, and nitrogen. In no case did these gases produce an arc frequency increase.

Our last experiment involved removal of the excess encapsulant along the solar cell edge. This was performed by soaking the solar cell in Dynasolve 220, a silicon solvent recommended by Dow Corning for their encapsulant(s). The solar cell was removed from the solvent and rinsed with methanol. The edges of the solar cell were inspected with the microscope.

The adhesive appeared removed, but liquid (either methanol or Dynasolve 220) remained trapped under the cover slip. Figure 10 presents a low magnification view of a cleaned edge. The cleaned solar cell was placed in the vacuum system for testing and pumped down to  $10^{-7}$  torr. Initially, this clean solar cell did arc, however, it exhibited a marked faster decline in arc frequency than for an uncleaned solar cell. After a 40-min bakeout, the solar cell could not be induced to arc. We now suspect this initial arcing was associated with trapped solvent. The inducements included: exposure to room air overnight and exposure to greater than  $2 \times 10^{-3}$  torr-min of  $H_2O$  vapor. Both of these treatments caused significant arc frequency increases on an uncleaned solar cell.



Figure 10. - Microscope picture of the cleaned edge of a solar cell.

### Experimental Conclusion

Moisture laden adhesive that may simultaneously come in contact with the space plasma and the high voltage base of a solar array will exhibit arcing phenomena at voltages more negative than -300V.

### Mitigation Strategies

Our findings confirmed at least one means of reducing arcing phenomena, but several others might be considered. Clearly elimination of the edge adhesive significantly reduces arcing frequency. This may be accomplished via several techniques, such as the solvent removal of the excess adhesive that we utilized above. We have investigated at least three other removal techniques including: pulsed water/methanol jet, high-speed rotary brush, and laser ablation. A continuous water jet at 300 psig through a  $650 \mu m$  orifice showed no substantial effects. Pulsed water/methanol/Dynasolve 210 jets showed only slight removal of the edge adhesive. In all cases the use of a solvent leads to lengthy drying times, i.e., days, and produces some undercutting of the adhesive layer between the cover glass and the silicon cell.

Laser ablation using a focused excimer laser beam at 193 nm,  $0.5 J/cm^2$  pulse and 25 Hz successfully removes the adhesive. However, great care must be utilized to mask the edge. This laser power is capable of ablating the silver base layers of the solar cell. Any higher power levels are capable of damaging even the UV transmitting cover glass material. Some charring may occur but typically wipes off with either  $H_2O$  or methanol. Times to ablate a 2 mm illuminated length of a solar cell edge required 30 to 60 seconds at the 25 Hz repetition rate.

High-speed rotary microbrushes are relatively successful. Custom fabricated brushes using one to three rows of roughly 100  $\mu\text{m}$  diameter wire bristles are recommended. Larger brushes can damage the corners of the solar cell, actually removing/rounding away the edge. Nylon brushes appear to have very little effect, and grinding stones or burrs are much too abrasive. Typical removal times are 30 to 60 seconds for a 2 cm length solar cell edge using a rotary speed of 10,000 rpm. A significant drawback for brushes occurs along the embedded interconnect edge. Great care must be used to avoid tearing or damaging the interconnect. Of course, for solar cells with unexposed interconnects located away from the cover slip edge, this issue is not a concern.

Arcing along the solar cell edge suggests the local electrostatic field contributes to the arc phenomena. This leads us to believe that a redesign of the cover glass edge geometry may help mitigate arc events. This redesign could be as simple as a larger overhang to protect the adhesive washout, however this leads to a size and weight penalty. Sloping or angled cover glass edges may be alternative approaches without associated weight penalties, however additional research must be conducted to verify these strategies.

The potentially best solution to the adhesive problem is new bonding technology. Currently efforts are underway to perfect and commercialize electrostatic or molecular bonding techniques to attach cover glass to the solar cell. It is our opinion that such a technique will significantly reduce arcing while possibly providing a weight savings.

#### Future Experiments

Our immediate efforts are to further document the arc frequency reduction and establish a threshold measurement technique/criteria. In addition, we are anxious to investigate the influence of plasma density, ion impact energy, and temperature on both the adhesive ladden and clean solar cells. Very soon we will have an electrostatic probe available to monitor the disposition of cover glass charge before and after an arc event. The most significant need is to investigate the arc initiation process. We also need to identify the microscopic role of water as an adsorbate and the adhesive as the arc propagator/carrier. We clearly need to identify any chemical/physical changes arising when adhesive, water, plasma are combined.

The authors would like to acknowledge technical assistance from Drs. David Sonnenfroh and Mark Allen, and helpful discussions with Drs. B.D. Green, A. Gelb, and Herb Cohen. We would also like to thank NASA Lewis Research Center for financial support through the SBIR program and Mr. Jim Albec of Spectralab Inc. for providing us with sample solar cells.

#### References

1. Kennerud, K.L.. 1974. High Voltage Solar Array Experiment, NASA Report CR-121280.
2. Synder, D.B.. 1984. Discharges on a Negatively Biased Solar Array, NASA TM-83644.
3. Synder, D.A.. 1984. Characteristic of Arc Currents on a Negatively Biased Solar Cell Array in a Plasma, NASA TM-83723, July.
4. Grier, N.T. 1983. Plasma Interaction Experiment II: Laboratory and Flight Results. 1983. Spacecraft Environment Interactions Technology Conference, Colorado, October 4-6, 1983, NASA CP-2359, p. 333-349.
5. Fujii, H., Y. Shibuya, T. Abe, K. Ljichi, R. Kasaia, and K. Kuriki. 1986. "Laboratory Simulation of Plasma Interactions with High Voltage Solar Arrays," Proceedings of the 15th International Symposium on Space Technology and Science, Tokyo.
6. Thiemann, H., and K. Bogus. 1986. ESA Journal, 10, 43-57.